

# Low-Cost, Underwater, Ultrasonic Phased Array Research Platform

Tejus Rao  
Engineering Department  
Harvey Mudd College  
Claremont, USA  
trao@hmc.edu

Alec Vercruyssen  
Engineering Department  
Harvey Mudd College  
Claremont, USA  
avercruyssen@hmc.edu

Rhea Zaverchand  
Engineering Department  
Harvey Mudd College  
Claremont, USA  
rzaverchand@hmc.edu

Matthew Spencer  
Engineering Department  
Harvey Mudd College  
Claremont, USA  
mspencer@hmc.edu

**Abstract**—This work presents an acoustic phased array that is open source and easy-to-modify. The phased array is intended to be used for marine biological ultrasound imaging research. The phased array costs 1710 USD, and this low cost was achieved by using off-the-shelf piezoelectric transducers and by building transmit and receive analog front ends using low-cost microcontrollers and analog pulse-shaping circuits. The array was characterized by measuring its radiation pattern and point spread function, and both of those measurements closely match theory. The transmit beam steering resolution is  $1.8^\circ$  and the receive beam steering resolution is  $0.5^\circ$ . The array was used to successfully capture an image of a static object 1.2 meters in front and 0.15 meters to the right of the array in a test tank.

**Index Terms**—ultrasound, phased-array, marine, underwater, image

## I. INTRODUCTION

Ultrasonic acoustic imagers are a common technology used for navigation and imaging underwater [1]. Acoustic imaging methods are often better suited to underwater vision applications than optical imaging because of the limitations of optical systems in low-light environments and dispersive media, though they offer limited resolution [1], [2]. For example, SONAR systems have been used for over a century in marine applications, leveraging acoustic frequencies between 100kHz and several megahertz for object recognition, localization, and data transmission, with lower frequencies used for longer range seafloor mapping [1], [3]. Ultrasound imaging has also been used in fishing and scientific monitoring [4], [5], and for tracking organisms, biodiversity mapping and animal behavior studies [6], [7].

Fortunately, ultrasound imagers have become made more accessible as low-cost ultrasound imaging research platforms have been proposed, but none of these platforms have been designed for underwater applications [8]–[10]. An ideal ultrasound imaging platform for marine biology would be waterproof, low-cost and easy-to-modify. Further, it would have a high frame rate (at least a few frames/second to track moving organisms), and a spatial resolution that can be tuned to match the size of the organism being studied.

Funding for this work was provided by the Rasmussen Summer Research Fund, the Rose Hills Foundation Grant, and the Sprague Experiential Learning Fund.

This paper presents an underwater acoustic phased array that is open source, low-cost, easy-to-modify, and suitable for use underwater. To reduce cost, this phased array uses commercially available transducers that were modified to increase power transfer between the transducer and water. Cost is further reduced by using low-cost microcontrollers to provide several crucial analog functions, including sampling data. This phased array has some limitations: grating lobes reduce the beam steering angle, and the frame rate is limited by the speed of an important data bus. Despite these limitations, the array has been used for simple object detection. The remainder of this paper provides the details of the array’s construction and test (Section II), the results of characterizing and testing the array (Section III), and concluding remarks (IV).

## II. METHODS

This work proposes an ultrasonic phased array consisting of a transducer array, channel circuitry – the transmit and receive interface circuitry for each transducer element – and a control computer that implements imaging algorithms. The physical design of the transducer array is introduced in section II-A. The channel circuitry is discussed further in section II-B. Finally, the beam forming and imaging algorithms implemented on the control computer are described in section II-C.

The components of the array are spread across several mechanical assemblies. The transducer array is one assembly. Each channel has its own assembly: a printed circuit board. The final assembly is a motherboard: a printed circuit board that connects nine channel boards to TX/RX switches and the transducer array.

### A. Physical Design

The transducer array in this work is a 3x3 array of American Piezoelectric (APC) 42-1012 cylindrical piezoelectric transducers, which have 1.6 cm diameters and 92 kHz resonant frequencies. The cylindrical piezoelectric transducers are packed into a uniform rectangular grid with a center-to-center spacing equal to the diameter of the transducer. The transducers are driven at resonance, which sets the emanated wavelength,  $\lambda$ , to 1.61 cm. That implies that the array spacing is  $\lambda$ , which introduces grating lobes into the beam pattern. The array is pictured in Figure 1a.

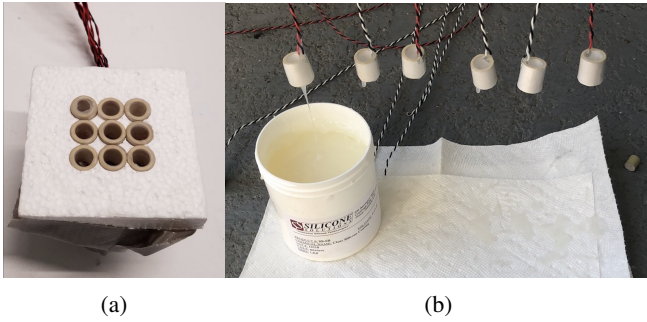


Fig. 1: (1a) Front view of the 3x3 piezoelectric element array. (1b) Each piezoelectric transducer was dipped into a container of Silicone Solutions SS-6B to improve acoustic impedance matching between the transducers and water.

The mechanical construction of the array affects its performance. The transducers are coated with a layer of Silicone Solutions SS-6B, as shown in Figure 1b, to enhance power transfer between the transducer and water. SS-6B is an effective anti-reflection coating because its impedance (1.4 Mrayl) is close to that of water (1.5 Mrayl). Because the silicone layer is thin and well adhered to the transducer, the entire transducer can be modeled as having an acoustic impedance close to that of water. This anti-reflection coating is applied using the following process: stranded leads, called contact wires, are attached to the inner and outer transducer walls using low temperature solder, then the whole transducer is dipped vertically into the silicone (such that the cylindrical opening is normal to the silicone surface) and hung in air to drip dry. The coated transducers are mounted to an acrylic back plate. The back plate provides mechanical support to the transducers, strain relief to the contact wires, and some improvement in directivity by preventing pressure waves from emanating from the back of the array. The transducers are also surrounded by a Styrofoam cutout to improve receive directivity.

### B. Channel Circuitry

The channel circuitry is made of two analog front ends (AFEs): a transmit (TX) AFE that drives the piezoelectric transducer, and a receive (RX) AFE that amplifies and filters signals reflected back onto the transducers. Figure 2 shows a block diagram of both AFEs.

The TX AFE creates high-voltage sinusoidal bursts. Figure 3 shows the voltage of the TX signal at each point in the multistage burst generator. The TX AFE can generate bursts with adjustable initial delays, burst amplitudes, and burst durations. When triggered by the rising edge of a digital signal called *sync*, the timer peripheral in each channel's microcontroller waits for an initial delay, then it generates a 92kHz square wave, typically with a 100  $\mu$ s duration, using the microcontroller's pulse-width modulation (PWM) peripheral. The resolution of the initial delay in this PWM signal sets the TX steering angle resolution of the array, which is  $1.8^\circ$  over the steering range. The PWM burst drives the select

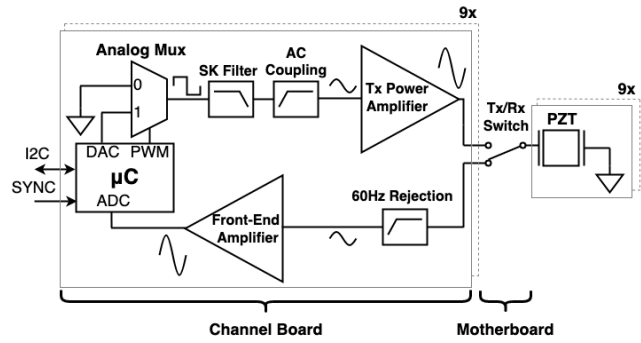


Fig. 2: Block diagram of analog front-end.

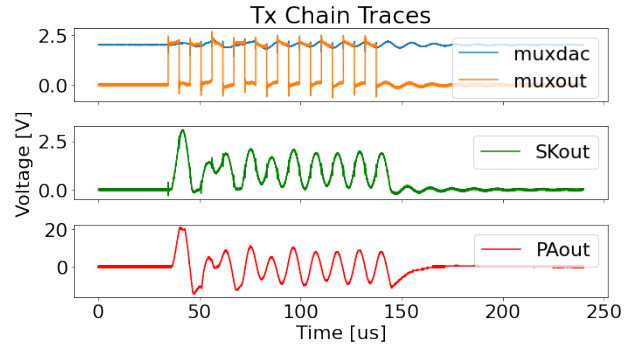


Fig. 3: Traces of an example transmission pulse at different points in the transmit analog front end.

line of an analog multiplexer, which causes the output of the multiplexer to switch between ground and a digital-to-analog converter (DAC) voltage. The DAC voltage, shown in figure 3 as the *muxdac* trace, is also generated by the channel microcontroller. The multiplexer output, shown figure 3 as the *muxout* trace, is driven into a set of amplifiers and filters that have a fixed gain of 31 dB. Because the amplifiers and filters have a fixed gain, the transmitted wave's amplitude is controlled by the DAC voltage.

One element of the TX AFE signal chain is a Sallen-Key low pass filter that is used to filter harmonics out of the multiplexer output. Removing these harmonics converts the output from a square wave to a sine wave. The *SKout* trace in Figure 3 shows the slow settling time of the filter during the first two periods of the burst. The output of the Sallen-Key filter is AC-coupled into a linear audio amplifier (the LM3886T), which amplifies the signal to a maximum voltage swing of  $\pm 40$ V. The output of this audio amplifier is shown by the *PAout* trace in Figure 3. The output of the amplifier is connected to a TX/RX switch, which in turn is connected to an element of the transducer array.

The RX AFE on each channel amplifies the signal with a high gain, then samples the signal coherently with the other channels. The first stage of the RX front-end is a first-order high-pass filter used for AC coupling and 60Hz rejection. The remaining stages comprise a multi-stage op-amp-based amplifier. The final stage of the voltage amplifier

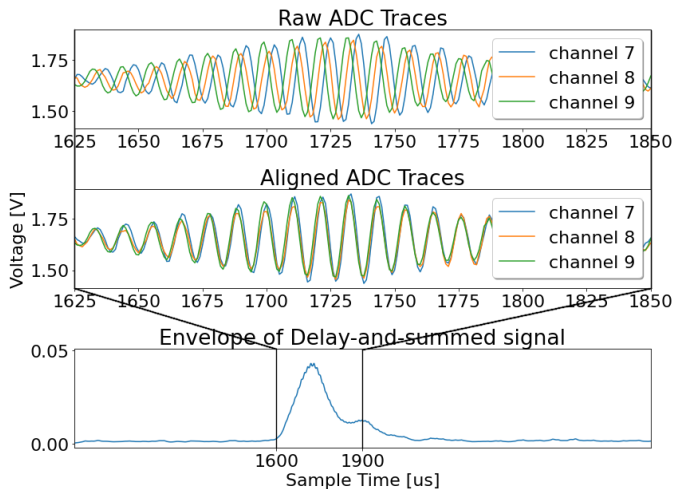


Fig. 4: Digital processing of three co-linear channels of a sampled signal. The bottom chart has a different time axis than the top two charts.

drives a series current limiting resistor, AC coupling capacitor, and voltage divider used to level shift the received signal to the 0-3.3V range. The RX AFE output is sampled at 1 MSPS by a 12-bit analog-to-digital converter (with 10.5 effective bits) embedded in the channel microcontroller. Each channel samples data using the same 1MHz clock in order to synchronize the samples. Sampling is enabled by the falling edge of the `sync` signal.

The duration of `sync` was configurable, and it was set to 800 us to delay sampling until the piezos stopped ringing after the transmit pulse. This sampling delay set the minimum range of the array to 0.742 m. Sampled data was stored in memory, then offloaded to the host computer for processing after sampling was completed.

### C. Imaging

The control computer constructs images one pixel at a time by using the TX and RX AFEs to affect both transmit and receive beamforming. Transmit beamforming sends ultrasonic energy in a direction, called the transmit angle, then sampled data is gathered on all channels as described in section II-B. The sampled data is upsampled by a factor of ten, then it is delayed and summed to maximize constructive interference of waves arriving from the transmit angle. The delayed-and-summed signal is half-wave rectified then low-pass filtered (i.e.: put through a software “diode-detector”) to produce a received intensity. An example of a received intensity signal, which has peaks corresponding to received echos, can be seen in figure 4.

The array is steered across a spherical coordinate system, gathering intensity data at each coordinate, to create an image. The coordinate system is bounded by a maximum angle, which was experimentally determined to be  $22.5^\circ$  using measurements discussed in III-A. Images are produced by mapping each intensity signal to a color space and plotting it at its

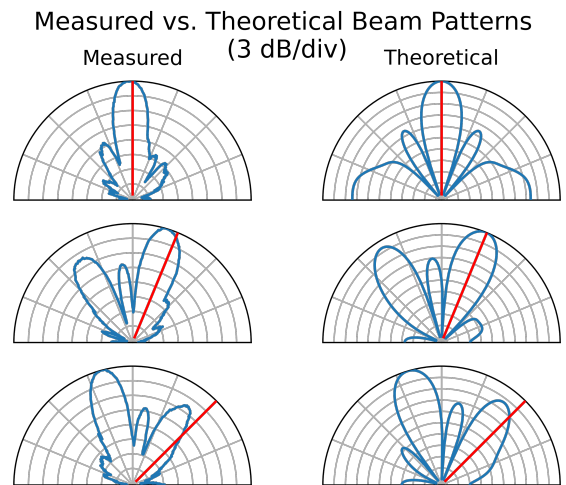


Fig. 5: Beam pattern measurements versus theory (conventional beamforming), for steering angles (in the positive  $x$  direction) of  $0^\circ$ ,  $22.5^\circ$ , and  $45^\circ$ .

spherical coordinate, where its radial coordinate is determined by estimating distance from time-of-flight. As needed, data was decimated or thresholded to improve the readability of the images.

This imaging algorithm relies on having all of the received data on the control computer, which ultimately limits the frame rate of this imager. Each channel is connected to the control computer through an I2C bus, which has a low (400 kbps) data rate, and each channel saves 40 kb of data each time it gathers samples, so offloading the data to the control computer takes 0.3 seconds per channel per coordinate.

## III. RESULTS AND DISCUSSION

The performance of the ultrasonic phase array was measured on the test range depicted in figure 7a. The radiation pattern and point spread function of the array are discussed in section III-A. A simple image measured using this array is discussed in section III-B.

### A. Array Characterization

The beam pattern (Fig. 5) in the horizontal plane was measured by mechanically rotating the array while the steering was held constant. The relative power of the beam at each angle was calculated from the maximum magnitude of the signal received by an Aquarian Scientific AS-1 hydrophone placed two meters away on the array’s broadside. The theoretical model was constructed using measurements of the beam pattern of an individual transducer.

Grating lobes are seen here because the array spacing was larger than  $\lambda/2$ . The steering angle of the array was reduced to  $22.5^\circ$  to avoid ambiguity from the grating lobes (as seen in Fig. 5). The power of the main lobe rapidly decreases beyond a steering angle of  $22.5^\circ$ , and the grating lobe is more powerful than the signal itself at a steering angle of  $45^\circ$ .

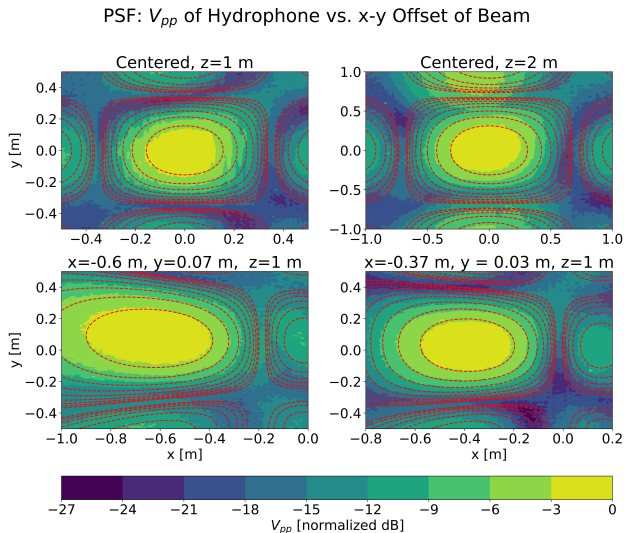


Fig. 6: Transmit Point Spread Functions (conventional beamforming). The 3dB contour lines of the theoretical point spread function of this system are displayed in red.

The point spread function of the transmitting beam, seen in Figure 6, demonstrates the size of the beam on x-y planes located 1 and 2 meters away from the array. The point-spread function was measured by aiming the array at points around a hydrophone using transmit beamforming as described in section II-C. The half-power beamwidth is seen as the brightest yellow contour on the figure. When the array is steered, the beamwidth appears to stretch because the x-y plane is no longer normal to the steering direction. Side lobes can be seen influencing the edges of each point spread function.

### B. Imaging Characterization

Figure 7b shows an optical image of a 30 cm  $\times$  16 cm steel plate in the water. The steel plate is seen  $x \approx 0.15$  m off the broadside axis of the ultrasound imager described in this work. The imager was used to capture 2D and 3D ultrasound renderings of this scene, which appear in figures 7c and 7b (respectively). The ultrasound images show the plate as a cluster of points at 1.2 meters away from the transducer array, which is represented by a red point. The cluster of points around the plate is larger than the plate itself because of the large size of the point spread function. The image could be improved with additional signal processing.

## IV. CONCLUSION

This paper presents a low-cost underwater acoustic phased array research system implemented with off-the-shelf piezoelectric transducers. This system offers control over transmit beam parameters, including burst amplitude, duration, and phase delay, which enables a variety of experiments. The channelized architecture of the transmit and receive circuitry allows the system to be easily scaled up to a 16- or 25-element array. Measurements and imaging algorithms are automated using a host computer. When tested as an imaging system with

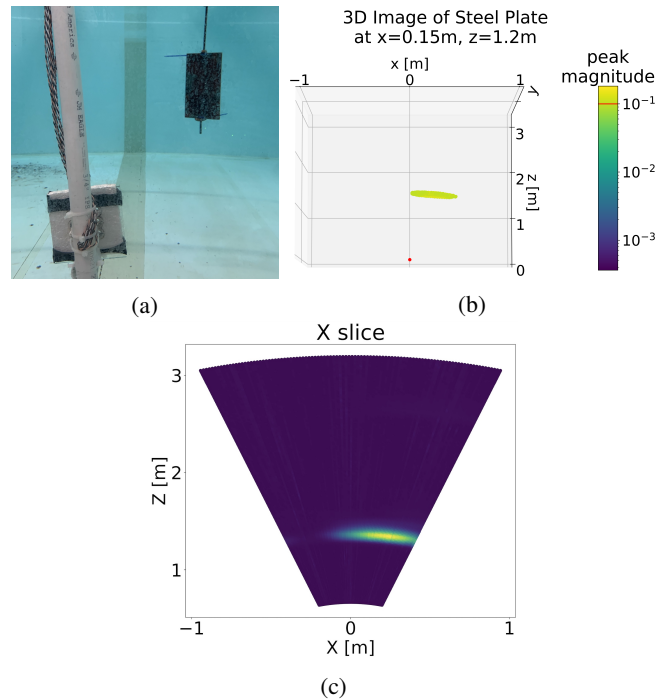


Fig. 7: Test setup used to capture images of metal plate submerged underwater and corresponding ultrasound images. The location of the phased array is plotted as a red point.

conventional delay-and-sum beamforming, this phased array successfully located a steel plate approximately 1.2 meters away. The cost of this system was only 1,710 USD, and it could be reduced to 1,200 USD by choosing different PCB manufacturers.

Ongoing work includes increasing the number of elements in the array, reducing the array spacing, improving data transfer rates between the channel and host computer, decreasing the size of the channel circuit boards, implementing signal processing algorithms to improve image quality, and deploying the system in biological monitoring applications.

## REFERENCES

- [1] V. Murino and A. Trucco, *Proc. of the IEEE*, vol. 88, no. 12, pp. 1903–1948, 2000.
- [2] F. Andreucci *et al.*, *IEEE Trans. on Ultrason., Ferroelect., and Freq. Control*, vol. 40, no. 6, pp. 805–813, 1993.
- [3] K. A. Ahmad *et al.*, in *2018 8th IEEE Int. Conf. on Control Syst., Comput. and Eng.*, pp. 233–237.
- [4] R. J. Korneliussen *et al.*, *Methods in Oceanogr.*, vol. 17, pp. 187–205, 2016.
- [5] D. N. MacLennan and D. V. Holliday, *ICES J. of Mar. Sci.*, vol. 53, pp. 513–516, 1996.
- [6] T. Porto Marques *et al.*, in *2021 IEEE/CVF Conf. on Comput. Vis. and Pattern Recognit. Workshops*, pp. 4373–4382.
- [7] T. Maki *et al.*, *Int. J. of Control, Automat. and Syst.*, vol. 18, no. 3, pp. 597–604, 2020.
- [8] C. Herickhoff *et al.*, in *2019 IEEE Int. Ultrason. Symp.*.
- [9] M. Fournelle *et al.*, in *2020 IEEE Int. Ultrason. Symp.*.
- [10] G. Allevato *et al.*, *IEEE Trans. on Ultrason., Ferroelect., and Freq. Control*, vol. 68, no. 3, pp. 796–806, 2021.